Unconventional myosin traffic in cells reveals a selective actin cytoskeleton

Crista M. Brawley and Ronald S. Rock[1]

Department of Biochemistry and Molecular Biology, The University of Chicago, 929 East 57th Street 60637, Chicago, IL 60637

Edited by Ronald D. Vale, University of California, San Francisco, CA, and approved April 17, 2009 (received for review October 16, 2008)

Eukaryotic cells have a self-organizing cytoskeleton where motors transport cargoes along cytoskeletal tracks. To understand the sorting process, we developed a system to observe single-molecule motility in a cellular context. We followed myosin classes V, VI, and X on triton-extracted actin cytoskeletons from *Drosophila* S2, mammalian COS-7, and mammalian U2OS cells. We find that these cells vary considerably in their global traffic patterns. The S2 and U2OS cells have regions of actin that either enhance or inhibit specific myosin classes. U2OS cells allow for 1 motor class, myosin VI, to move along stress fiber bundles, while motility of myosin V and X are suppressed. Myosin X motors are recruited to filopodia and the lamellar edge in S2 cells, whereas myosin VI motility is excluded from the same regions. Furthermore, we also see different velocities of myosin V motors in central regions of S2 cells, suggesting regional control of motor motility by the actin cytoskeleton. We also find unexpected features of the actin cytoskeletal network, including a population of reversed filaments with the barbed-end toward the cell center. This myosin motor regulation demonstrates that native actin cytoskeletons are more than just a collection of filaments.

actin cytoskeleton | myosin motors | single-molecule

Myosins are a large family of structurally diverse molecular motors that are the basis of many cellular movements including neurite outgrowth, phagocytosis, vesicle and organelle trafficking, formation of stereocilia in sensory hair cells, cell migration, cytokinesis, and maintenance of cell shape (1–4). In addition to the conventional class of myosin motors (class II) that drive muscle contraction and cytokinesis, many classes of unconventional myosin motors are expressed throughout numerous eukaryotic cell types (4). All myosins share a conserved domain that binds to filamentous actin and hydrolyzes ATP to produce movement along actin. Of the few unconventional myosins that have been studied, many have been found to be processive motors that take multiple mechanical steps and hydrolyze multiple ATPs before releasing from their actin track. This processivity allows single myosin motor molecules to walk along actin using its head domain to interact with actin while transporting cargo to a destination with its tail domain. Thus, like the highly processive kinesin and dynein motors that move along microtubules, myosin can transport cellular cargoes over large distances.

Cells carefully regulate these unconventional myosins to transport cargoes and organize their cellular contents. However, at the molecular level, we are only beginning to understand how myosin motors navigate a dense and complex actin cytoskeleton. In certain cases, actin-binding proteins (ABPs) such as tropomyosins can decorate subpopulations of actin filaments. A few myosin motors are known to identify and walk along these tropomyosin-decorated filaments in preference to other filaments (5). Other motors recognize the spatial arrangement of actin (6). These 2 studies highlight a critical need to understand how motors recognize their actin tracks in vitro and in vivo to move cargo throughout the actin cortex. Unfortunately, traditional in vitro motility assays fall short for this purpose in that the ABPs and the native actin architecture that encode the cellular roadmap are absent.

We developed a strategy that allows us to perform motility assays on intact cellular cytoskeletal actin with full biochemical control of the assay conditions. In this technique, which we call the *ex vivo* motility assay, we gently detergent extract the plasma membrane from live, unfixed, adherent cells while simultaneously stabilizing the actin networks with rhodamine-phalloidin. We then perfuse labeled myosin motors under motility conditions. Imaging is performed with TIRF (total internal reflection fluorescence) or near-TIRF (7, 8) microscopy to track individual motors. Our sample preparation is similar in some respects to the triton cytoskeletons that have been used to measure force transduction and protein binding to actin (9, 10). The Sheetz group found that these triton extracted cells retain the ability to interact with signaling components in a tension-sensitive manner; therefore, observing myosin motor motility on these preserved actin architectures should be physiologically relevant. We find that perforation of the plasma membrane in this *ex vivo* motility assay carries 2 key advantages: first, we can unambiguously identify the start and end of processive motor runs since motors can diffuse away from the dense array of actin filaments; and second, motors uniformly sample the cellular actin as they continuously escape and are replenished without concentrating in any given region of the cell.

Results

We examined each of 3 classes of myosin (V, VI, and X) on 3 distinct cell lines (S2, COS-7, and U2OS). The 3 cell types were selected because they exhibit 3 separate examples of actin organization; the motors were selected as examples of motor species that move in different directions and prefer different actin substrates (e.g., actin bundles vs. filaments). All 3 cell lines spread to form thin cells that are ideal for TIRF or near-TIRF microscopy, and kinesin motor behavior has already been analyzed in COS-7 cells (11, 12). The actin architecture and protein composition is preserved in our detergent extracted cells (Figs. S1–S3). There is ample actin visible throughout the cell body of all cells as well as throughout the lamella and filopodia, when present (Fig. S2). These actin networks in extracted cells appear similar to fixed cells stained with phalloidin (Fig. S2). Furthermore, we do not see any significant difference in protein composition between extracted cells and unextracted cells (Fig. S1 *A* and *B*). Together, we conclude that the cells are relatively intact and structurally comparable to live cells.

Directly following extraction, we observed 3 different classes of Cy5-labeled myosin motors (13) moving on the preserved cytoskeletons in the presence of ATP. For now, we use heavy meromyosin (HMM) fragments of myosin V (MV), myosin VI (MVI), and myosin X (MX). These fragments lack the cargo-

Author contributions: C.M.B. and R.S.R. designed research; C.M.B. performed research; C.M.B. and R.S.R. contributed new reagents/analytic tools; C.M.B. and R.S.R. analyzed data; and C.M.B. and R.S.R. wrote the paper.

The authors declare no conflict of interest.

This article is a PNAS Direct Submission.

[1]To whom correspondence should be addressed. E-mail: rrock@uchicago.edu.

This article contains supporting information online at www.pnas.org/cgi/content/full/0810451106/DCSupplemental.

Table 1. Comparison of *Drosophila* S2, COS-7, and U2OS cells for MV, MVI, and MX

	Drosophila S2	COS-7	U2OS	Myosin
Moving motors	26% (138/540)	17% (144/832)*	4% (30/668)*	V
Velocity (μm/s)	0.36 ± 0.08 (SD)	0.42 ± 0.19 (SD)	0.41 ± 0.20 (SD)	
Track switching	5% (7/138)	15% (22/144)*	27% (8/30)	
Run length (μm)	0.85 ± 0.06 (SE)	1.03 ± 0.06 (SE)	0.30 ± 0.06* (SE)	
Moving motors	17% (196/1144)**	8% (126/1544)*,**	8% (128/1688)*,**	VI
Velocity (μm/s)	0.33 ± 0.11 (SD)	0.36 ± 0.21 (SD)	0.25 ± 0.08 (SD)	
Track switching	10% (20/196)	8% (10/126)	6% (8/128)	
Run length (μm)	0.81 ± 0.07 (SE)	0.34 ± 0.03* (SE)	0.39 ± 0.06* (SE)	
Moving motors	5% (203/4412)**	7% (59/873)**	3% (24/772)	X
Velocity (μm/s)	0.58 ± 0.21 (SD)	0.73 ± 0.29 (SD)	0.41 ± 0.17 (SD)	
Track switching	8% (17/203)	42% (25/59)*	8% (2/24)	
Run length (μm)	0.81 ± 0.09 (SE)	0.63 ± 0.10 (SE)	0.26 ± 0.03 (SE)	

*, Significant difference at the $\alpha = 0.05$ level (across cell types, compared to S2 cells). **, Significant difference in the fraction of moving motors at the $\alpha = 0.05$ level, compared to myosin V. Run lengths tested using the Kolmogorov–Smirnov test. The Bonferroni correction was applied to the reported α to correct for multiple testing.

binding tail-domains to avoid complications with motors that are only active with bound cargo. Except for a few runs that abruptly change direction (see below), all runs move in nearly straight lines (Movies S1–S9). To verify straight trajectories over a larger number of frames, we imaged MVI motility in COS-7 cells at a 10× faster frame rate (0.05-s exposure). These TIRF movies enabled us to track moving MVI motors over 8–85 frames (0.4–4.4 s) and obtain velocities similar to that previously found in COS-7 cells at saturating ATP (0.35 ± 0.16 μm/s, $n = 50$; compare to Table 1). Since this faster frame rate analysis yielded straight runs (Fig. S5) with the same velocity, we conclude that we are not mistakenly identifying "diffusive" events as linear motor runs. As a further test to exclude diffusive events, we show that motor velocities are ATP dependent. Under limiting ATP concentrations (1 μM), our MVI motors moved more slowly in S2 (0.21 ± 0.07 μm/s, $n = 13$), COS-7 (0.21 ± 0.07 μm/s, $n = 23$), and U2OS cells (0.10 ± 0.04 μm/s, $n = 11$; compare to Table 1).

We constructed trajectory maps that show each processive run as an arrow superimposed on an image of the extracted cell. As expected, we see largely radial traffic of MV and MVI in S2 cells (Fig. 1), while MX concentrates on filopodia and the lamella edge (Fig. 2). On COS-7 cells, we see largely isotropic motion of each motor, while U2OS cells support moderate MVI motility but little motility of MV and MX (Fig. 3). Our observed velocities and run lengths (Table 1, Figs. S4 and S6) are the same as in TIRF in vitro motility assays (6, 14–16), with a few exceptions that are discussed below.

To determine the directionality of each motor run we define an orientation angle (θ) for each straight trajectory. The angle θ is the angle of the motor trajectory vector, with respect to the vector from the cell centroid to the starting point of the trajectory (Fig. 1*A*). Orientation angles near 180° indicate runs toward the cell periphery; angles near 90° are circumferential runs; and orientation angles near 0° indicate runs toward the cell center. We excluded trajectories with an internal bend of at least 20° from this analysis, as these runs likely represent motility along 2 or more filaments. This orientation analysis is most useful in the S2 cells; we show motor orientations in these cells in Figs. 1 *C* and *F* and 2 *D*–*F*. Trajectory orientation angles in COS-7 and U2OS cells are found in Fig. S7.

We cannot exclude the possibility that certain regions of these cells are less accessible to motor runs, either due to remnants of plasma membrane or due to dense upper strata of actin filaments that block access to the lower regions. However, we note that motor landing events occur throughout the cells and that motor run lengths are generally comparable to those that we observe in vitro.

Discussion

Motor Traffic Patterns Reveal the Actin Network Architecture. Myosin V and myosin X both move toward the barbed end of actin filaments (17, 18) while myosin VI moves toward the pointed end (19). Therefore, we may use our *ex vivo* motility assay to dissect cellular actin architecture, as a motor trajectory reports the location and polarity of the underlying filament without ambiguity. The general features of actin organization are clearest in the *Drosophila* S2 cells. This macrophage-like cell line spreads on concanavalin-A surfaces to yield thin, circular cells (20). The circular symmetry of this cell type is apparent from the MV and MVI trajectory maps and orientation angles (Fig. 1 *B*, *C*, *E*, and *F*). Of the motors taking straight processive runs, MV generally moves to the cell periphery while MVI generally moves toward the interior. These directions are consistent with the known orientation of actin-barbed ends toward the plasma membrane (21–23). Although processive MV runs become less likely as the orientation angle decreases (and vice versa for MVI), in each case roughly 10% of the runs travel in the opposite direction with a similar velocity. This surprising motility of MV toward the cell center and MVI toward the periphery suggests that at least some actin filaments are reversed, with their barbed ends toward the cell center. This population of reversed filaments may be as high as 10%, but can be lower if these cells also contain a large population of inert actin filaments that do not support myosin motility, which would effectively dilute the reversed filament population. It is possible that the actual population of reversed filaments is sufficiently small that they have been missed in prior EM and fluorescence studies. We propose that these reversed filaments may be used in a return traffic pathway to move cargo in the opposite direction with the same motor.

Previously, we have shown that myosin X is highly processive on bundled actin filaments (6) like those found in filopodia (24). Because filopodia are bundled by the actin-bundling protein fascin (25, 26), which is encoded by *singed* in *Drosophila* (27), we analyzed extracted cells that displayed filopodia (Fig. 2*A*). Here, we find 3 categories of MX directionality in S2 cells. First, we find MXs that move radially outward along filopodia, with an orientation angle near 180° ($n = 46/184$, 25%; $\theta_{min} = 107°$; Fig. 2 *C* and *D*). We also find MXs that travel along the cell circumference around the lamella edge, with a corresponding orientation angle near 90° ($n = 34/184$, 18%; $\theta_{min} = 55°$, $\theta_{max} = 120°$; Fig. 2 *C* and *E*). Tokuo et al. also observed motility of myosin X clusters along the cell edge, where it is likely involved in reorganizing circumferential fascin-actin bundles into filopodial projections (28, 29). The remainder of MX runs occurs through-

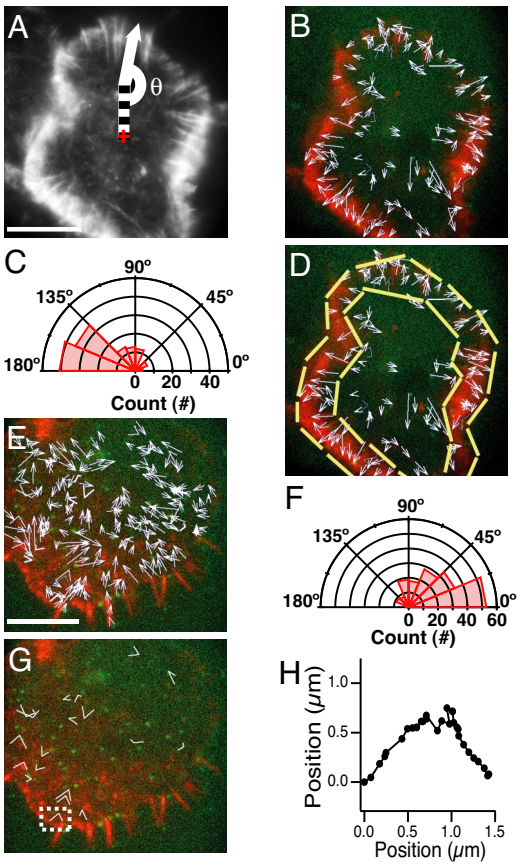

Fig. 1. Myosin V and VI motility on the actin cytoskeleton of extracted Drosophila S2 cells. (*A*) Preserved actin cytoskeleton in an extracted S2 cell visualized via rhodamine-phalloidin. The center point of the cell is indicated (+, red). The angle θ is defined as the orientation angle and measured from the centroid of the cell to the beginning of a motor run (arrow). (Scale bar, 10 μm.) (*B*) Trajectory map (white arrows) of all myosin V motor (green) runs on the preserved actin cytoskeleton (red). Each arrow represents a single moving motor run. A processive run is defined as a linear movement lasting at least 3 consecutive frames (≥ 1.5 s). Each frame is acquired with a 0.5-s exposure for 200 frames. The majority of motors (76%) move toward the cell periphery. Very few MV motors (n = 7/138) actually switch actin tracks throughout this analysis (cyan). (*C*) Orientation angle measurements for processive runs. The majority of MV motors have a trajectory angle of 100–180°, indicating that the motors move toward the cell periphery. (*D*) The zone of motility (yellow outline) is where most motors move toward the cell periphery with a similar velocity. This motility zone is directly adjacent to a central zone of slow motility. (*E*) Trajectory map (white arrows) of single myosin VI motors (green) moving on a preserved actin cytoskeleton (red). Each arrow represents a single motor run. The majority of motors (72%) move away from the cell periphery. (Scale bar, 10 μm.) (*F*) Orientation angles measured for all MVI motors making a processive run. Most motors have a trajectory angle of 0–80°, indicating that these motors move away from the cell periphery or toward the cell center. (*G*) MVI motors that switch actin tracks are depicted (white). There are more MVI motors that switch than MV motors (compare to panel *B*, cyan). (*H*) Tracking pattern of a MVI motor that switches actin tracks (boxed in *G*). The motor runs for 26 frames over a distance of 1.5 μm. Since this motor tracks with a sharp turn (>20°), it is characterized as a motor that switches actin tracks during motility.

out the cell body on actin structures that are difficult to distinguish due to the density of filaments (n = 104/184, 57%; Fig. 2*F*). This last set of runs does not show a preferred direction. MX motors making runs on filopodia and around the lamella move at an average velocity of 0.58 ± 0.21 μm/s (± SD, n = 26; Fig. S3), with an unusually broad distribution compared to MV and MVI (Table 1). This velocity is 2 times faster than we

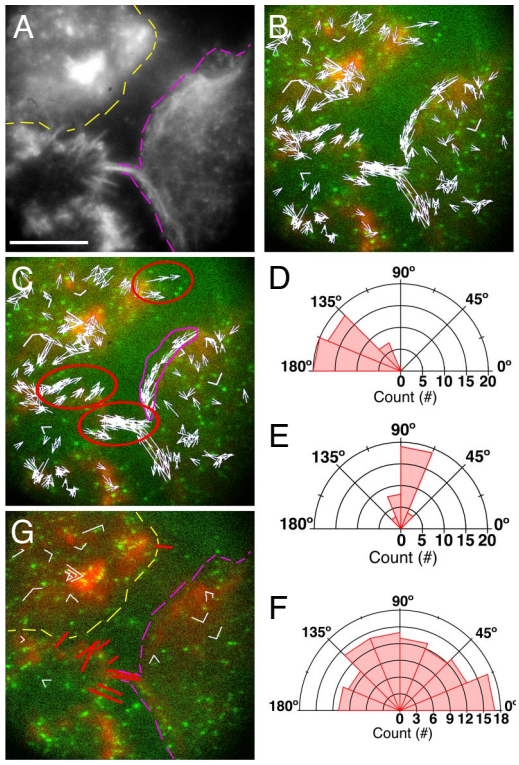

Fig. 2. Myosin X motors move on filopodia and around the lamella edge of permeabilized Drosophila S2 cells. (*A*) Multiple extracted S2 cells displaying filopodia, lamella edge (purple dotted line) and a cell edge (yellow dotted line). The actin cytoskeleton is visible with TMR-phalloidin. (Scale bar, 10 μm.) (*B*) Trajectory map (white arrows) of all moving MX motors throughout these cells. (*C*) MX motors that make runs on filopodia (red circles) and around the lamella edge (magenta) move at various velocities (Fig. S6) on this bundled actin. (*D–F*) Orientation angle measurements for all moving MX motors. Motors moving on filopodia (*D*) have a center angle of 100–180°, indicating that motors start at the base of filopodia and run out, toward the cell periphery. Center angles determined for motors moving on the lamella (*E*) indicated that these motors move circumferentially at an angle of 55–120°. All other motors moving throughout the cells revealed an uncorrelated center angle measurement (*F*), indicating that these motors move in all directions. (*G*) Some MX motors switch tracks (white) while making a run. These track switching events do not occur on the filopodia (red lines), the lamellar edge (purple dotted line), or at the cell edge (yellow dotted line).

observed previously in vitro (6), suggesting that filopodial MX events in the *ex vivo* motility assay are on more organized bundles.

Unlike the trajectories in S2 cells, myosin motility in the fibroblast COS-7 cell line is far more isotropic, with all motors showing runs sampling all orientation angles (Fig. S7). This suggests a lack of the global actin organization apparent in S2 cells, although we cannot rule out more locally organized arrays of actin. However, we do not observe large populations of runs that align with obvious actin bundles or stress fibers. In the osteosarcoma cell line U2OS, we see little motility of any sort (discussed further below). The most active motor, MVI, seems to track along the prominent stress fibers that are found in this cell line (Fig. 3 and Fig. S7).

When presented with a high density of crossed actin filaments, myosin motors can switch actin filament tracks in the middle of a processive run and travel in a new direction. We define a track-switching event as a trajectory with an internal bend of at least 20°, and infer that the motor switched filaments when such a sharp bend is observed (e.g., Fig. 1*H*). A single actin filament is unlikely to bend over these short lengths. Using this criterion,

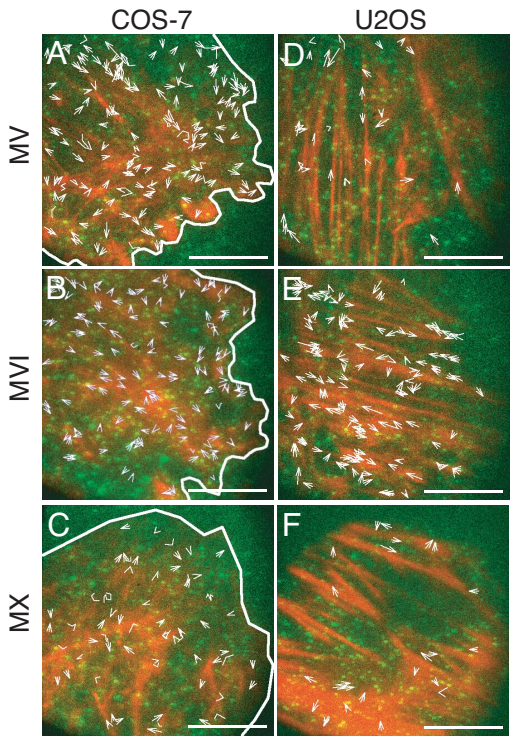

Fig. 3. Myosin V, VI, and X motility on extracted mammalian COS-7 and U2OS cells. Trajectory maps of moving myosin motors. MV runs in COS-7 (*A*) and U2OS (*D*) cells. MV motors in both cells move with the same velocity (Table 1 and Fig. S6), but considerably fewer runs are made in U2OS (*D*) compared with COS-7 (*A*) cells. MVI runs in COS-7 (*B*) and U2OS (*E*) cells. MVI motors move at a similar velocity and run length (Fig. S6 and Table 1) in both COS-7 and U2OS cells. Although, MVI runs track along the large stress fibers that run the length of U2OS cells (*E*). MX runs in COS-7 (*C*) and U2OS (*F*) cells. Few MX runs are detected in COS-7 cells, but even fewer are detected in U2OS cells. (Scale bars, 10 μm.)

we generally find that 5–15% of motors switch tracks within a processive run (Table 1). But MV has been suggested to switch actin tracks with nearly a 50% probability at crossed filaments that are in direct contact (30, 31). We propose that cellular actin filaments, although crowded, have sufficient separation to inhibit this track-switching behavior. Curiously, we found that track switching is particularly common for MX motors in COS-7 cells for unknown reasons (Table 1).

With 1 notable exception, we find run lengths comparable to the in vitro values for all motors across all cell types that exhibited significant runs (i.e., excluding the rare MV and MX runs on U2OS, see below) (Table 1, Fig. S4). Thus, the cellular actin architecture neither enhances nor inhibits processivity. Since our runs are generally straight, with few track-switching events, it seems likely that runs begin and end on the same filament. Thus, the motors must walk along filaments that are longer, on average, than the observed run length, or about 1–1.5 μm on S2 and COS-7 cells. Although a parallel bundle of short actin filaments could serve as a potential substitute, these did not enhance the processivity of myosin V in vitro (6). Surprisingly, we found an unusually long run length of 0.81 $\pm$ 0.07 μm ($\pm$ SE, n = 196; Fig. S4) for MVI in S2 cells. This run length is 3 times longer than observed previously in vitro (15), suggesting that the architecture of actin within these preserved cells enhances processive MVI runs. One possibility is that an unknown actin-ABP complex promotes myosin VI motility, much like fascin does for myosin X (6). Since MVI seems to run along stress fibers in U2OS cells, stress fibers may present a favored architecture for MVI. Curiously, MVI run lengths drop significantly from S2 to COS-7 cells, while the run lengths for the other 2 motors are nearly the same in these 2 cell lines (Table 1 and Fig. S4). This implies that in the COS-7 cells, myosin VI moves along a distinct population of actin. These actin filaments are either shorter or have roadblocks that disrupt processive motility.

Regioselective Motility of Myosins. We also found ample evidence for regioselective motility, where motor activity is modulated from region to region across a single S2 or U2OS cell. As discussed above, in S2 cells with prominent filopodia and circumferential fascin-actin bundles, we find nearly half of the MX events in these narrow zones (Fig. 3). Surprisingly, we find that myosin VI is excluded from the same regions. In the S2 cell shown in Fig. 1*E*, only 1 filopodium out of 11 supports MVI motility (n = 3 motor events) even though numerous motors land on the other filopodia. We believe this filopodium has a unique feature that allows MVI motility, since statistically there is only a 1:121 probability that all 3 events would occur on 1 filopodium (i.e., the probability that 2 subsequent events occurred on the same filopodium as the first event). One possibility is that there are general features of filopodial actin that exclude MVI, but these features have been lost from the single filopodium. Alternatively, the other 10 filopodia may have remnants of plasma membrane that block all motors, but we note that we still observe MVI landing events on these filopodia, and that myosin X walks into filopodia and is able to escape at the tips under the same conditions. Even though MVI is apparently excluded from filopodial fascin-actin bundles, it does seem to walk along α-actinin bundles found in stress fibers (Fig. 3).

Even more surprisingly, we find that motor velocities can vary across the surface of a single cell. For MV in S2 cells shown in Fig. 1*B*, the motors move at a velocity of 0.36 $\pm$ 0.08 μm/s ($\pm$ SD, n = 138), while the subset of motors in the center of the cell move slower (0.17 $\pm$ 0.09 μm/s, $\pm$ SD, n = 25) (Fig. 1*D* and Fig. S4). The S2 cells are thicker in the center, but a cosine error from oblique actin filaments cannot account for a 2-fold difference in velocity, since we do not observe the motor moving out of focus. Previously published in vitro TIRF velocities for MV agree with the faster motors at the periphery (14, 32). Thus, it seems that some feature of the central actin is either inhibiting the rate-limiting ADP release step (33, 34), or introducing a new rate-limiting process without significantly affecting the MV run length. Alternatively, the arrangement of actin filaments in the central region may force MV to take a shorter step, with unaltered kinetics.

The COS-7 cells provide a counterexample of cells that lack apparent regioselectivity, as they display uniform motility of all 3 motors across the entire cell surface (Fig. 3). Any regioselective motility that does exist in a COS-7 cell must be confined to small areas that are effectively randomized over the whole cell and not immediately apparent in our assay.

Class-selective Motor Regulation Across Cell Types. We also found evidence that each cell line differentially regulates global myosin motor traffic, distinguishing between motor classes. We find that both S2 and COS-7 cells support active MV motility, reflected in the fraction of motors that move once they have landed on the cellular actin. We find a lower likelihood that MVI moves in these cells, and MX is the least likely to move (although the difference is insignificant between MVI and MX in COS-7 cells). Although all of these motors likely play multifaceted roles, the general trend is that vesicle traffic (MV) (35) dominates over organelle anchoring and endocytosis (MVI) (36), followed by integrin or filopodial traffic (MX) (37). U2OS cells show a different pattern, with moderate levels of MVI motility, and a statistically significant reduction of MV and MX motility.

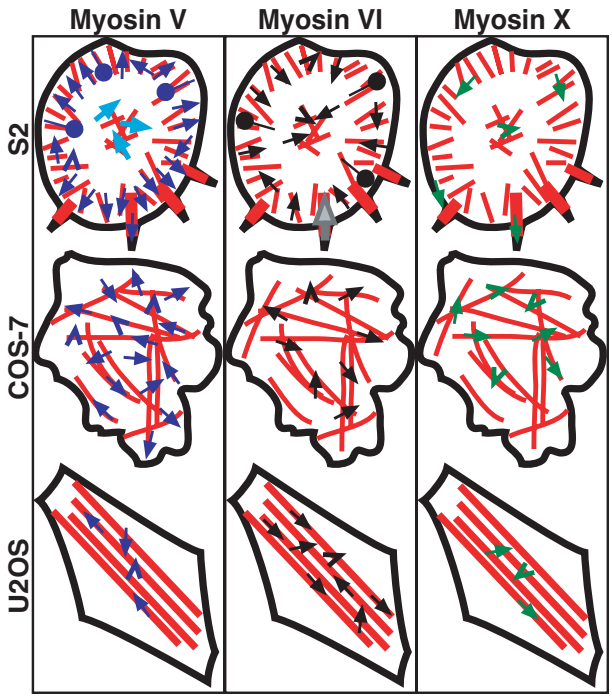

Fig. 4. Summary of unconventional myosin tracking in S2, COS-7, and U2OS cells. A cartoon of the spatial arrangement and properties of actin filaments or bundles in the 3 cell types examined here. The number of symbols displayed in each cell is directly proportional to the percentage of moving motors in that cell type (1 symbol = 1%). An arrow indicates a motor run. A lollipop arrow indicated a run in the opposite direction than expected. Chevrons indicate motors that switch tracks. MV motors in S2 cells show the highest percentage of moving motors compared to all cell types. These MV runs are primarily directed toward the cell periphery, but a percentage of motors do run toward the cell center (lollipop arrows). Runs that are made in the center of the cell move at a slower velocity (light blue arrows) than those made in the outer cortical region of the cell. There are also a good percentage of moving MV motors in COS-7 cells. These runs are not as directed as in S2 cells and are throughout the cell. In U2OS cells, few MV runs are seen. MVI motors in S2 cells primarily track toward the cell center, but a fraction move toward the cell periphery (lollipop arrows). A few runs are also found on a single filopodium (gray arrow). Isotropic MVI runs are seen in COS-7 cells, but fewer than MV. In U2OS cells, MVI is the primary moving motor. MVI makes significantly more runs than MV or MX on stress fiber bundles. MX takes the fewest runs in every cell type. In S2 cells, MX motors travel on filopodia and around the lamellar edge as expected, but overall MX makes significantly fewer runs than MV and MVI. Track-switching behavior was observed throughout this analysis, with the most track-switching behavior exhibited by MX in COS-7 cells.

Conclusions

Cells tightly regulate the assembly and disassembly of actin, resulting in specific changes in morphology and cell motility. Our results here suggest that the details of cellular actin organization also impact the activity of unconventional myosins. Using this information on myosin motor motility, we can now construct a map of the roads or actin structures in different cell types, as shown in Fig. 4. This roadmap reveals both the spatial arrangement of the actin filaments, as well as the individual motility preferences in the 3 cell types. We note that the 2 cell types that support the most myosin traffic, S2 and COS-7 cells, are likely to have the greatest requirements for intracellular trafficking. The process of an S2 cell spreading on a concanavalin-A surface has been described as a frustrated attempt to phagocytose the surface (20, 38). Such a cell would need to actively traffic integrins and other receptors to and from the plasma membrane. Likewise, an actively migrating fibroblast such as a COS-7 cell would likely have active trafficking pathways for cell migration. Both of these cell types have active actin polymerization at the lamellopodium, with retrograde flow rates of approximately 4 μm/min determined by speckle microscopy (39). Ostap has proposed that this pool of new dynamic actin filaments can select for certain myosin classes such as myosin Ib, since inhibitory tropomyosins are not found in regions with rapid filament turnover (40). Our myosins may prefer these regions as well for similar reasons. In contrast, the slowly migrating U2OS cell maintains prominent stress fibers and is well-anchored to the substrate, with correspondingly low actin retrograde flow rates at the leading edge ($\approx$0.25 μm/min) (41). The ability of myosin VI to move along U2OS stress fibers may reflect this motor's role in the load-dependent anchoring (42) of organelles such as the Golgi (36) rather than active trafficking. Since we used the same motor constructs on all 3 cell lines, these motors are most likely regulated at the level of the underlying actin architecture. Our future work will identify the actin roadblocks and detour signs that control the flow of motor traffic, in part through the siRNA-mediated depletion of ABPs that are potential players in this system.

Materials and Methods

Protein Constructs and Expression. The myosin X HMM forced dimer construct containing GCN4, GFP, and FLAG (6) was used to create recombinant baculovirus in Sf9 insect cells, purified via Flag-affinity chromatography. Myosin V and myosin VI HMM-GCN4-GFP-Flag constructs were likewise expressed and purified in Sf9 cells using baculovirus expression system as previously described (15). Motor stock concentrations were determined from GFP absorbance. Exchange reactions with Cy5-labeled calmodulin were performed by a calcium pulse as previously described with a 3-fold molar excess of labeled calmodulin over myosin (13).

Extraction Method. *Drosophila* S2 cells were plated on concanavalin-A coated coverslips and allowed to adhere for 1 h to overnight at room temperature. COS-7 and U2OS cells were plated onto coverslips and allowed to adhere for 12–48 h at 37 °C. Coverslips were treated with extraction mixture [0.25–1% Triton X-100 (Calbiochem), 4% wt/vol PEG, PEM buffer (100 mM Pipes, pH = 6.9, 1 mM $MgCl_2$, and 1 mM EGTA), and 1 μM TMR-phalloidin] for 2–5 min. Longer adherence time typically allowed for higher detergent concentration without loss of cell adhesion. Treated coverslips were assembled into a flow cell comprised of 2 microscope slide fragments used as spacers adhered to a microscope slide with double stick tape (chamber volume $\approx$170 μL). Motility solution containing myosin motors, ATP (2 mM or 1 μM with 3 mM free Mg^{+2}), and an oxygen scavenging system (25 μg/mL glucose oxidase, 45 μg/mL catalase, and 1% wt/vol glucose) were washed into the flow cell and sealed with VALAP (equal weight of lanolin, Vaseline, and paraffin). Treated S2, COS-7, and U2OS coverslips were also subjected to hot (95 °C) SDS/PAGE sample buffer (60 mM Tris-HCl, pH = 6.8, 25% (wt/vol) glycerol, 0.01% (wt/vol) bromophenol blue, and 1 mM 2-mercaptoehtanol). Collected samples were heated at 95 °C for 5 min, loaded onto 4–20% SDS/PAGE gradient gels (Pierce), and subjected to SDS/PAGE (Fig. S1).

Single Molecule Imaging. Myosin motility was imaged using a custom-built objective-type total internal reflection microscope. Images were collected with a 100×, 1.45 NA objective (Olympus and Zeiss) and an EMCCD camera (iXon, Andor Technologies). Illumination intensities were 11.6 W/cm^2 at 532 nm (TMR) and 15.4 W/cm^2 at 633 nm (Cy5). Frames were collected at 2 Hz with a pixel size of 60 nm. Actin was imaged first and then excitation was promptly switched to the motor channel to image motility. Overlaying the actin image with the motility movie facilitated the identification of moving motors on actin within cells. We imaged 3–4 cells per coverslip and analyzed 2–20 cells per cell type per motor class. We identified moving spots by eye and then tracked them by eye and verified selective runs with spot-tracker in ImageJ (43, 44). Data for spots that moved $<$1.5 sec was discarded from analysis to eliminate misidentified diffusive events. We tested for observer bias by having a third-party tabulate movies of U2OS cells with MX motors as a blind trial. When we compared trajectory maps, 95% of the runs were found in both sets, with few differences in runs (missed events n = 3/64; track-switching differences n = 3/64). Near-TIRF movies were also collected and analyzed as above (7, 8). With NTIRF the incidence angle is not totally internally reflected to enable a larger image depth within the

sample (≈500 nm). We estimate that trajectory angular resolution is ± 3°. Faster frame rate movies were also acquired as above in COS-7 cells with MVI. These movies were acquired with a 0.05-s exposure for 200 frames. Fifty (25/movie) random runs were tabulated ranging from 8–85 frames in length. We imaged at 23 °C.

ACKNOWLEDGMENTS. The authors would like to thank Doug Robinson for useful comments on the manuscript, and the Rock lab for technical assistance. The project described was supported by grant number T32CA009594 from the National Cancer Institute (C.B.) and National Institutes of Health Grant GM078450 (R.S.R.).

1. Bahler M (2000) Are class III and class IX myosins motorized signalling molecules? *Biochim Biophys Acta* 1496:52–59.
2. Sellers J (1999) in *Myosins* (Oxford University Press, Oxford).
3. Berg JS, Powell BC, Cheney RE (2001) A millennial myosin census. *Mol Biol Cell* 12:780–794.
4. Tuxworth RI, Titus MA (2000) Unconventional myosins: Anchors in the membrane traffic relay. *Traffic* 1:11–18.
5. Tang N, Ostap EM (2001) Motor domain-dependent localization of myo1b (myr-1). *Curr Biol* 11:1131–1135.
6. Nagy S, et al. (2008) A myosin motor that selects bundled actin for motility. *Proc Natl Acad Sci USA* 105:9616–9620.
7. Tokunaga M, Imamoto N, Sakata-Sogawa K (2008) Highly inclined thin illumination enables clear single-molecule imaging in cells. *Nat Methods* 5:159–161.
8. Konopka CA, Bednarek SY (2008) Variable-angle epifluorescence microscopy: A new way to look at protein dynamics in the plant cell cortex. *Plant J* 53:186–196.
9. Sawada Y, Sheetz MP (2002) Force transduction by Triton cytoskeletons. *J Cell Biol* 156:609–615.
10. Brown S, Levinson W, Spudich JA (1976) Cytoskeletal elements of chick embryo fibroblasts revealed by detergent extraction. *J Supramol Struct* 5:119–130.
11. Cai D, Verhey KJ, Meyhofer E (2007) Tracking single Kinesin molecules in the cytoplasm of mammalian cells. *Biophys J* 92:4137–4144.
12. Hammond JW, Griffin K, Jih GT, Stuckey J, Verhey KJ (2008) Co-operative versus independent transport of different cargoes by Kinesin-1. *Traffic* 9:725–741.
13. Churchman LS, Okten Z, Rock RS, Dawson JF, Spudich JA (2005) Single molecule high-resolution colocalization of Cy3 and Cy5 attached to macromolecules measures intramolecular distances through time. *Proc Natl Acad Sci USA* 102:1419–1423.
14. Sakamoto T, et al. (2003) Neck length and processivity of myosin V. *J Biol Chem* 278:29201–29207.
15. Rock RS, et al. (2001) Myosin VI is a processive motor with a large step size. *Proc Natl Acad Sci USA* 98:13655–13659.
16. Okten Z, Churchman LS, Rock RS, Spudich JA (2004) Myosin VI walks hand-over-hand along actin. *Nat Struct Mol Biol* 11:884–887.
17. Sellers JR, Goodson HV (1995) Motor proteins 2: myosin. *Protein Profile* 2:1323–1423.
18. Homma K, Saito J, Ikebe R, Ikebe M (2001) Motor function and regulation of myosin X. *J Biol Chem* 276:34348–34354.
19. Wells AL, et al. (1999) Myosin VI is an actin-based motor that moves backwards. *Nature* 401:505–508.
20. Rogers SL, Wiedemann U, Hacker U, Turck C, Vale RD (2004) Drosophila RhoGEF2 associates with microtubule plus ends in an EB1-dependent manner. *Curr Biol* 14:1827–1833.
21. Small JV, Isenberg G, Celis JE (1978) Polarity of actin at the leading edge of cultured cells. *Nature* 272:638–639.
22. Pollard TD, Borisy GG (2003) Cellular motility driven by assembly and disassembly of actin filaments. *Cell* 112:453–465.
23. Symons MH, Mitchison TJ (1991) Control of actin polymerization in live and permeabilized fibroblasts. *J Cell Biol* 114:503–513.
24. Berg JS, Cheney RE (2002) Myosin-X is an unconventional myosin that undergoes intrafilopodial motility. *Nat Cell Biol* 4:246–250.
25. Vignjevic D, et al. (2006) Role of fascin in filopodial protrusion. *J Cell Biol* 174:863–875.
26. Aratyn YS, Schaus TE, Taylor EW, Borisy GG (2007) Intrinsic dynamic behavior of fascin in filopodia. *Mol Biol Cell* 18:3928–3940.
27. Cant K, Knowles BA, Mooseker MS, Cooley L (1994) Drosophila singed, a fascin homolog, is required for actin bundle formation during oogenesis and bristle extension. *J Cell Biol* 125:369–380.
28. Sousa AD, Cheney RE (2005) Myosin-X: A molecular motor at the cell's fingertips. *Trends Cell Biol* 15:533–539.
29. Tokuo H, Mabuchi K, Ikebe M (2007) The motor activity of myosin-X promotes actin fiber convergence at the cell periphery to initiate filopodia formation. *J Cell Biol* 179:229–238.
30. Ross JL, Ali MY, Warshaw DM (2008) Cargo transport: Molecular motors navigate a complex cytoskeleton. *Curr Opin Cell Biol* 20:41–47.
31. Ali MY, et al. (2007) Myosin Va maneuvers through actin intersections and diffuses along microtubules. *Proc Natl Acad Sci USA* 104:4332–4336.
32. Baker JE, et al. (2004) Myosin V processivity: Multiple kinetic pathways for head-to-head coordination. *Proc Natl Acad Sci USA* 101:5542–5546.
33. De La Cruz EM, Wells AL, Rosenfeld SS, Ostap EM, Sweeney HL (1999) The kinetic mechanism of myosin V. *Proc Natl Acad Sci USA* 96:13726–13731.
34. Rief M, et al. (2000) Myosin-V stepping kinetics: A molecular model for processivity. *Proc Natl Acad Sci USA* 97:9482–9486.
35. Cheney RE, et al. (1993) Brain myosin-V is a two-headed unconventional myosin with motor activity. *Cell* 75:13–23.
36. Buss F, Spudich G, Kendrick-Jones J (2004) Myosin VI: Cellular functions and motor properties. *Annu Rev Cell* Dev Biol 20:649–676.
37. Bohil AB, Robertson BW, Cheney RE (2006) Myosin-X is a molecular motor that functions in filopodia formation. *Proc Natl Acad Sci USA* 103:12411–12416.
38. Rogers SL, Rogers GC (2008) Culture of Drosophila S2 cells and their use for RNAi-mediated loss-of-function studies and immunofluorescence microscopy. *Nat Protoc* 3:606–611.
39. Rogers SL, Wiedemann U, Stuurman N, Vale RD (2003) Molecular requirements for actin-based lamella formation in Drosophila S2 cells. *J Cell Biol* 162:1079–1088.
40. Ostap EM (2008) Tropomyosins as discriminators of myosin function. *Adv Exp Med Biol* 644:273–282.
41. Hotulainen P, Lappalainen P (2006) Stress fibers are generated by two distinct actin assembly mechanisms in motile cells. *J Cell Biol* 173:383–394.
42. Altman D, Sweeney HL, Spudich JA (2004) The mechanism of myosin VI translocation and its load-induced anchoring. *Cell* 116:737–749.
43. Abramoff MD, Magelhaes PJ, Ram SJ (2004) Imaging processing with ImageJ. *Biophotonics International* 11(36).
44. Sage D, Neumann FR, Hediger F, Gasser SM, Unser M (2005) Automatic tracking of individual fluorescence particles: Application to the study of chromosome dynamics. *IEEE Trans Image Process* 14:1372–1383.